공학석사학위논문

PI Controller Design and Aeroservoelastic Analysis of a Smart Fin Including Piezoelectric Actuator for Performance Improvement

성능 개선을 위한 압전재료 구동 지능형 조종익의 PI 제어기 설계 및 서보공력탄성학 해석

2016년 8월

서울대학교 대학원

기계항공공학부

강 유 진

PI Controller Design and Aeroservoelastic Analysis of a Smart Fin Including Piezoelectric Actuator for Performance Improvement

성능 개선을 위한 압전재료 조종익의 PI 제어기 설계 및 서보공력탄성학 해석

지도교수 신상준

이 논문을 공학석사 학위논문으로 제출함

2016년 8월

서울대학교 대학원

기계항공공학부

강 유 진

강유진의 석사학위논문을 인준함

2016년 8월

위 원 장 _____ (인)

부 위 원 장 _____ (인)

위 원 _____ (인)

Abstract

PI Controller Design and Aeroservoelastic Analysis of a Smart Fin Including Piezoelectric Actuator for Performance Improvement

Yoojin Kang

Mechanical and Aerospace Engineering

The Graduate School

Seoul National University

For a lighter aerial vehicle, an actuator made of smart material such as piezoelectric material can be used to operate a control surface. The piezoelectric material in the actuator can adjust the pitch angle of the control surface by being transformed due to voltage difference, and the control surface of such type is called the smart fin. In the present paper, starting from the fundamental structural analysis, the aeroelastic and aeroservoelastic stability, and structural response simulations of the smart fin control system are performed by integration of MSC.NASTRAN, ZAERO and MATLAB/Simulink. In the process, PI controller is designed to ensure the flight stability and to maintain the pitch angles of the smart fin under a specific flight conditions. And then, the complete closed-loop control system of the smart fin is constructed and analyzed in both ZAERO and MATLAB/Simulink. The controllers develop the flight and control performances by increasing the flutter boundary and decreasing settling time of the step responses of the smart fin.

Keywords: Smart Fin, Piezoelectric Material, Rational Function Approximation, Aeroelasticity, Flutter, Aeroservoelasticity, PI controller, MATLAB/Simulink, ZAERO, Modal Analysis

Student Number: 2014-22507

List of Contents

List of Figures

List of Tables

I. Introduction

1.1 Backgrounds and Motivations

1.1.1 Backgrounds of Aeroservoelasticity

As aerial vehicles attempt more efficient mission accomplishments, they feature lighter and flexible structures. Flexibility of the structures induces complexity in the aerodynamic characteristics of the aerial vehicles and brings unexpected instability phenomena. Elastic deformation of the flexible structure generates additional complicated aerodynamic forces, and such aerodynamic forces will act on the structures again. This influence is studied in the field of aeroelasticity. In 1946, Collar constructed the interaction cycle by forming the triangle diagram, shown in Figure 1.1 [1-2]. The formulation of the aeroelastic equations of the flexible aerial vehicle was set for the first time by Ashley [3] in 1962.

Since the advent of flutter, which is a deadly phenomenon due to the interaction between the inertial and elastic forces of structures and the aerodynamic forces around the structures, there have been many researches about the aeroelaticity. Flutter is a representative aeroelastic instability phenomenon, and this triggers fatal destruction of aerial vehicle by generating oscillatory amplification on it, and the flight speed at that time is called the flutter speed. . Flutter implies unstable potential so that it may be

required to analyze the aeroelastic stability in the phase of design of all the aerial vehicles.

Most of the aerial vehicles have control surfaces like aileron, flap, elevator and rudder for maintaining or changing the flight attitudes. Those control surfaces, attached to aerial vehicle, influences on the airflow around the vehicle by generating control forces. Adding the control forces to the Collar's triangle diagram [1], the interaction between control dynamics and aeroelastic characteristics may be important, and this is studied in the field of aeroservoelasticity [5]. In other words, aeroservoelasticity handles the interaction among the inertial, elastic forces from structures, unsteady aerodynamics and control forces. There have been also lots of researches on aeroservoelasiticy of aerial vehicle including the control system. Historically, Garrick [6] observed the aeroelastic response by applying active flutter control of an aerial vehicle with external stores. In one of those researches about aeroservoelastic analysis, Mehmet explained that it would be possible to apply control theory for designing controller to stabilize the flight when the state-space equations of the aeroservoelastic system are established [5]. Aeroservoelastic structural time responses can be extracted by providing the state-space equations, and this offers the stability results. Aeroservoelasticity considers control forces, and is also vital area for almost modern aerial vehicle having control surfaces and control systems. Actually, related research, was performed by Mehmet, which is about aeroservoelastic analysis of a high speed vehicle control fin [5]. Mehmet modeled

an aeroservoelastic closed-loop diagram of the high speed vehicle fin (Figure 1.2), and the fin control system is composed of an actuator, rotational spring and a trapezoidal fin (Figure 1.3). From the structural analysis, to be specific, modal analysis, aeroelastic stability, actuator modeling and aeroservoelstic structural responses of the complete high speed vehicle control fin were performed by using MSC.NASTRAN, MSC.FlightLoads and MATLAB/Simulink, respectively. The research flow and used commercial calculating programs in the paper are depicted in Figure 1.4.

1.1.2 Backgrounds of Smart Structures

Since 1900s, control surfaces have been equipped on wings of aerial vehicle for the purpose of maneuver or resistance to external disturbances. The control surfaces are operated by using actuator system like hinge, hydraulic mechanical system, servo motors and even linkage. The actuator systems resemble the wire and linkage attached to the Flyer made by Wright brothers who succeeded to fly for the first time. These actuator systems, however, occupy space and increase total weight and size of aerial vehicle so these systems may be able to decline the aerodynamic performances. From this motivation, developed actuation system has been introduced. The developed actuation system derives from birds, shape-changing wings. Smart materials can deform by themselves to generate moments and change the wing shapes. Eventually, the aerial vehicle can maneuver the flight attitudes by changing the wing shape like a

bird. Development of these smart materials containing piezoelectric materials has been progressed in research and experiments for better physical properties, like long endurance, lighter weight, and fatigue property, etc. For example, Yoon designed an actuator including a piezo single crystal ceramic, called PMN-29PT. PMN-29PT has relatively larger piezo-electric constant (d_{31}) than CTS 3203HD does, which is made of poly crystaline ceramic. The actuator by PMN-29PT, produces 1.6 times more tip deflection than a conventional lightweight piezo ceramic actuator (LIPCA) with CTS 3203HD [7]. Piezoelectricity is electric charging in a material in response to external mechanical stresses, and the materials are called piezoelectric materials, involved in the class of smart materials [8]. Considering it opposite, it is discovered that strain is proportional to the applied voltage into the piezoelectric material, leading to be widely used as roles of sensors as well as actuators. [9]. Structures equipping smart materials are called the smart structures or the intelligent structures. The actuator system composed of smart materials has several advantages. One of those advantages is the space saving, because there is no need to equip additional parts such as hinge, linkage, servo motors, force transmission devices and hydraulic system [10-11]. Saving the space is very important for small aerial vehicle [11]. However, the application of smart materials to aerial vehicles is limited, because the actuator using smart materials is expensive and relatively more brittle [12]. The actuator including smart materials has complexity in the design due to their hysteresis phenomenon. Thus, many researches about smart materials in various area. Regarding application examples, Barrett [10]

made a torque plate composed of piezoelectric material, which produces the pitch deflection of $\pm 3°$ of an aerodynamic shell. The test of the pitch deflection of the aerodynamic shell including the torque plate in a wind tunnel at speed up to 50 m/s is performed and the torque plate produces the pitch deflection of $\pm 2.2°$ in a wind tunnel at speed of 40 m/s, as shown in Figure 1.6 [10]. Another application of a piezoelectric macro fiber composite (MFC) actuators onto a micro air vehicle (MAV), is performed by Ohanian [13]. Ohanian compared the designed morphing control surface, depicted in Figure 1.7, with a servo-actuated flapped airfoil by proposing the characteristics of aerodynamics of them. The experimental results showed that the morphing control surface has superior aerodynamic performances as shown in Figure 1.8. Moreover, the subjects of the comparison between them involve the size, weight, and even the actuation bandwidth during cycle testing and lastly the reliability.

1.1.3 Motivations of Present Thesis

In recent research, combining the main two subjects, the smart material and aeroservoelasticity, there have been many researches about applications of piezoelectric material on aerial vehicles and further aeroservoelastic analysis of the vehicles. One of those was performed by Sahin [14]. Smart fin with sixteen piezoelectric plates was studied for aeroservoelastic analysis. The sixteen piezoelectric plates were used to change the shape of the fin, leading to maneuver the flight attitudes, as shown in Fig

1.8. Sahin observed time simulations while sensing displacement of the specific area, by using a piezoelectric plate, as well. Furthermore, H-infinity controller and μ-synthesis controller were designed to stabilize the system of the smart fin. Eventually the system was stabilized and controlled by piezoelectric materials [14].

1.2 Objectives of the Present Thesis

A smart fin including an actuator composed of piezoelectric material is being studied for its ultimate requirements. The ultimate requirements is to control of flight dynamics with the flight speed of up to Mach 0.6, as following and maintaining the pilot input of the pitch angle of the smart fin, within 0.1 second. For the control, the smart fin needs to be deformed in pitch angle of 10°, and the piezoelectric actuator is actuated by applied voltage with the limit of 450 Voltages. However the piezoelectric actuator, which has developed until now, does not actually produce the pitch angle of 10°. Meanwhile, the purpose of this thesis is to propose the methodology of the construction of a closed-loop control system of the smart fin, for the pitch angle of the smart fin to follow and maintain the pilot input with the flight speed of up to Mach 0.6, and respond to the pilot input within 0.1 second. With the piezoelectric actuator, the smart fin is analyzed in many fields of study, from the structural analysis to the ASE analysis in the present thesis. For getting the plant of the closed-loop control system, containing the structures and aerodynamics of the smart fin control system, MSC.NASTRAN and

ZAERO are used. With the plant, controllers are designed for increasing the flutter boundary of the smart fin, and for decreasing the settling time of the structural responses of the pitch angle versus the pilot input, by using ZAERO and MATLAB/Simulink, respectively. Finally, the closed-loop control system with designed controller is compared to the open-loop system, which contains only the plant.

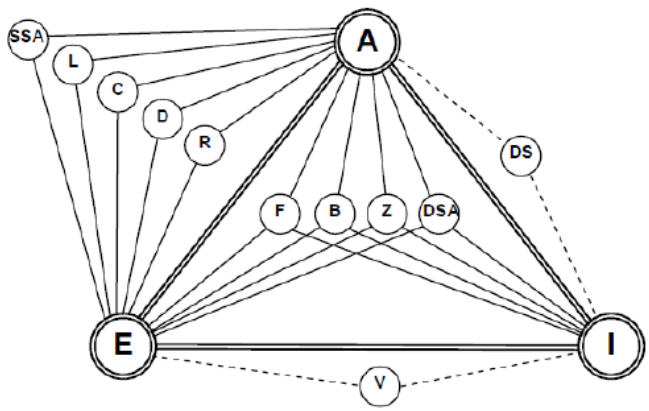

A: Aerodynamic forces
E: Elastic forces
I: Inertia forces

Related Fields
V: Mechanical vibrations
DS: Dynamic stability

Static Aeroelastic Phenomena
SSA: Aeroelastic effects on static stability
L: Load distribution
C: Control effectiveness
D: Divergence
R: Control system reversal

Dynamic Aeroelastic Phenomena
F: Flutter
B: Buffeting
Z: Dynamic response
DSA: Aeroelastic effects on dynamic stability

Figure 1.1 Collar's Triangle Diagram [1]

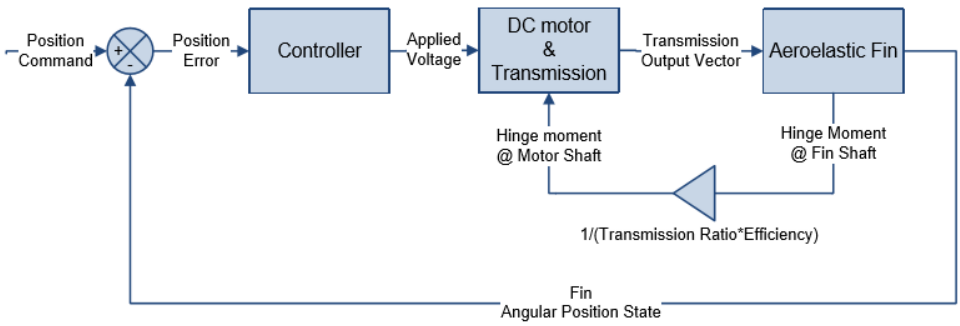

Figure 1.2 Aeroservoelastic Modeling of a Missile Control Fin [5]

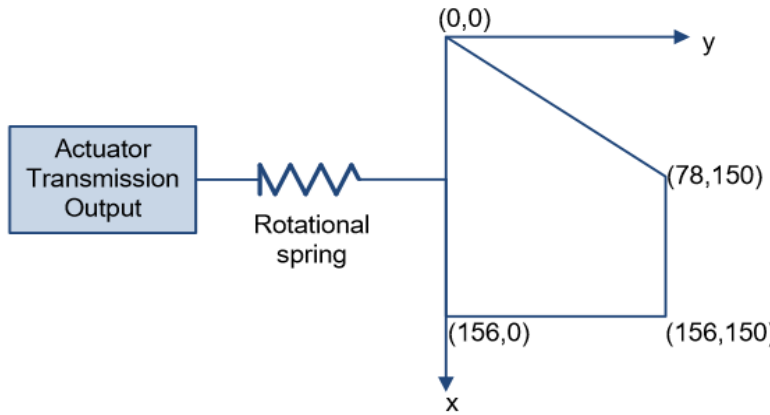

Figure 1.3 Structural Model of a Missile Control Fin [5]

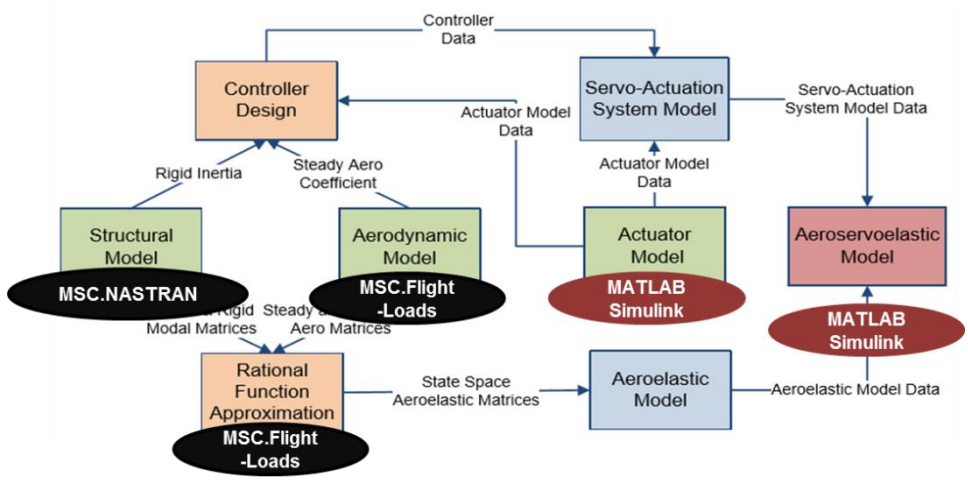

Figure 1.4 Research Flow and Commercial Program

Used by Mehmet [5]

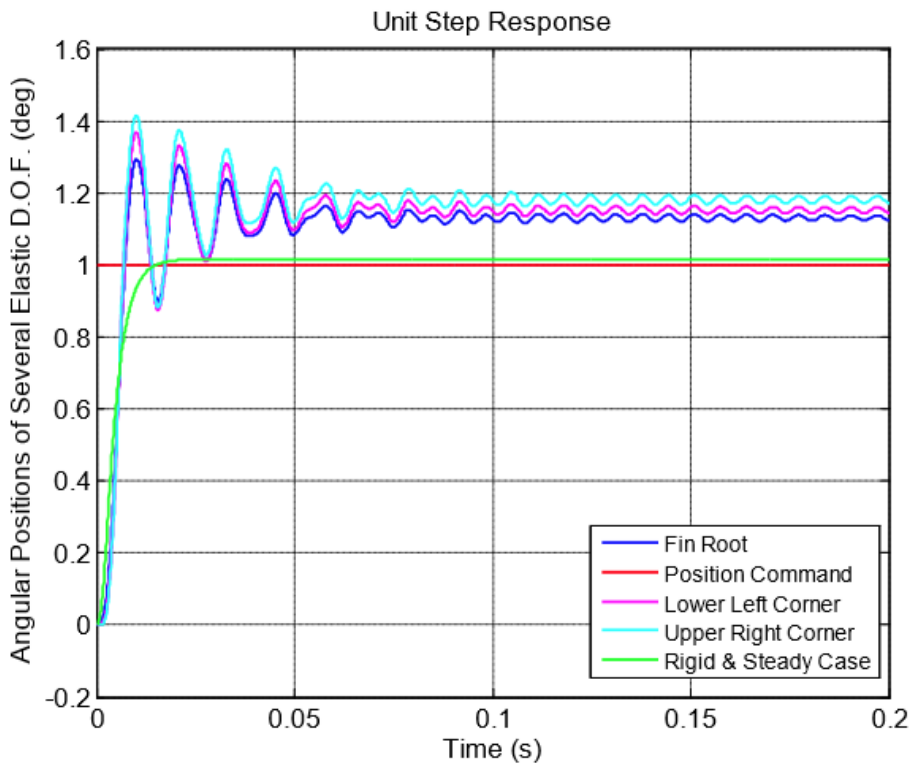

Figure 1.5 Aeroservoelastic Structural Responses in MATLAB/Simulink by Mehmet [5]

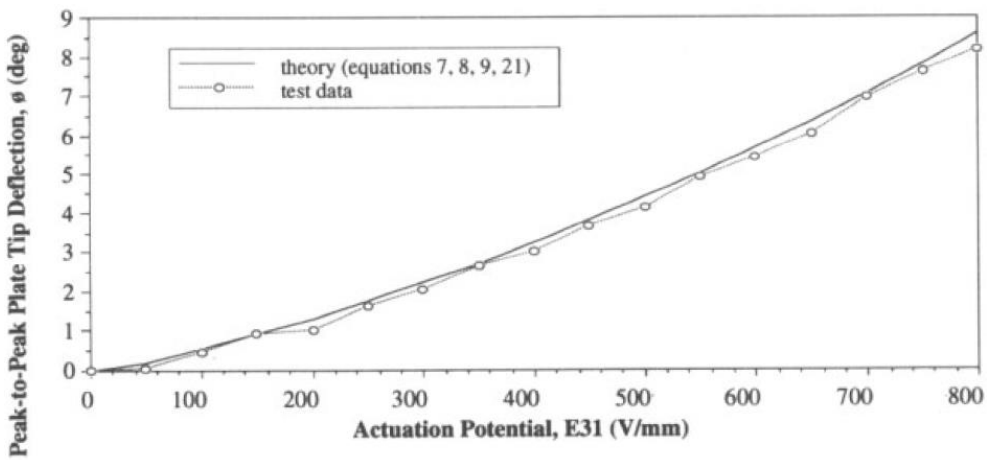

Figure 1.6 DAP Torque Plate Twist Prediction and Experiment [10]

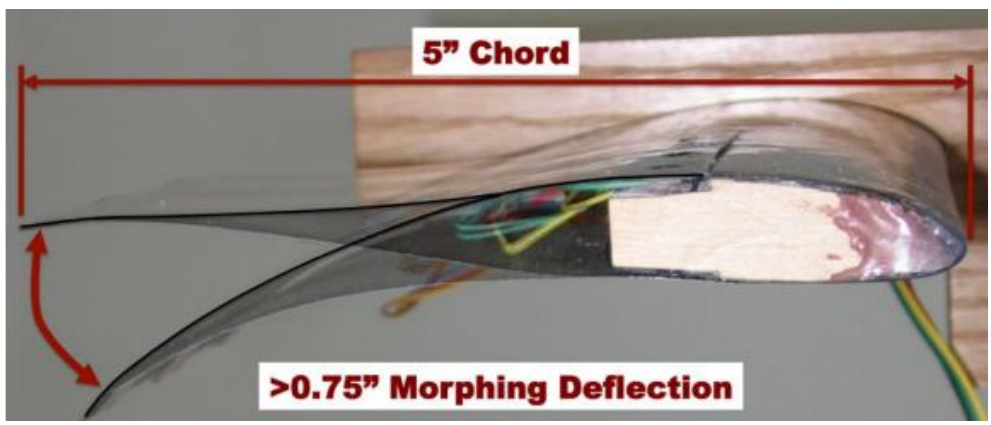

Figure 1.7 Prototypes of a Morphing Airfoil with Embedded MFC Actuators [12]

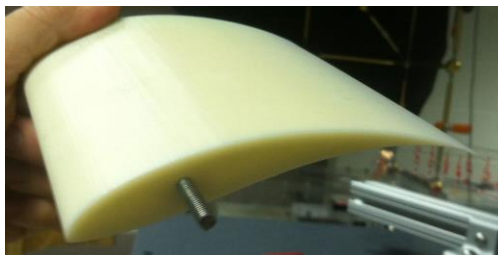

(a) Continuous Morphed Profile

(b) Discontinuous Flap

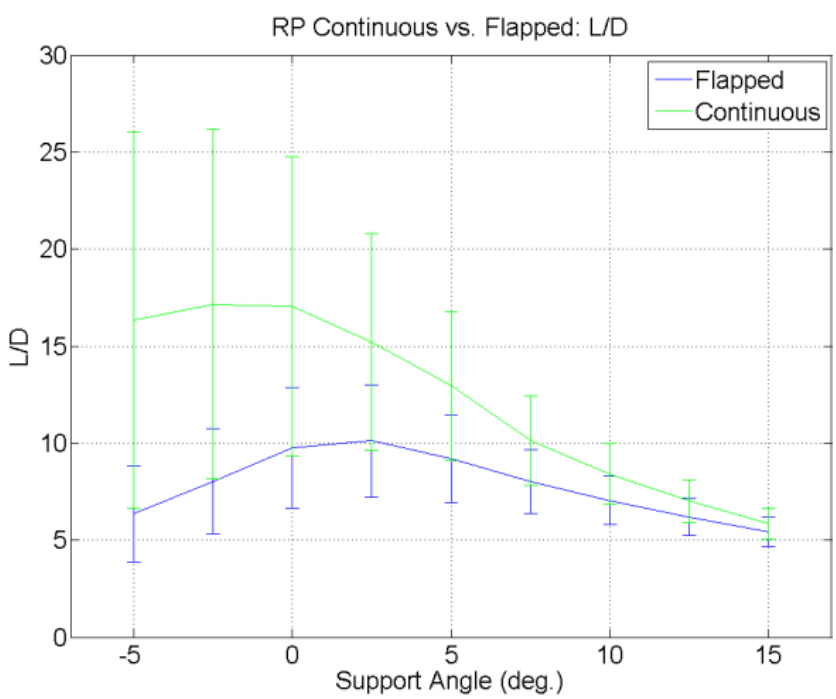

(c) Plot of the Lift to Drag Ratio as a Function of Support Angle

Figure 1.8 Fabricated Airfoils and the Lift to Drag Ratio for both Continuous and Flapped Airfoils [12]

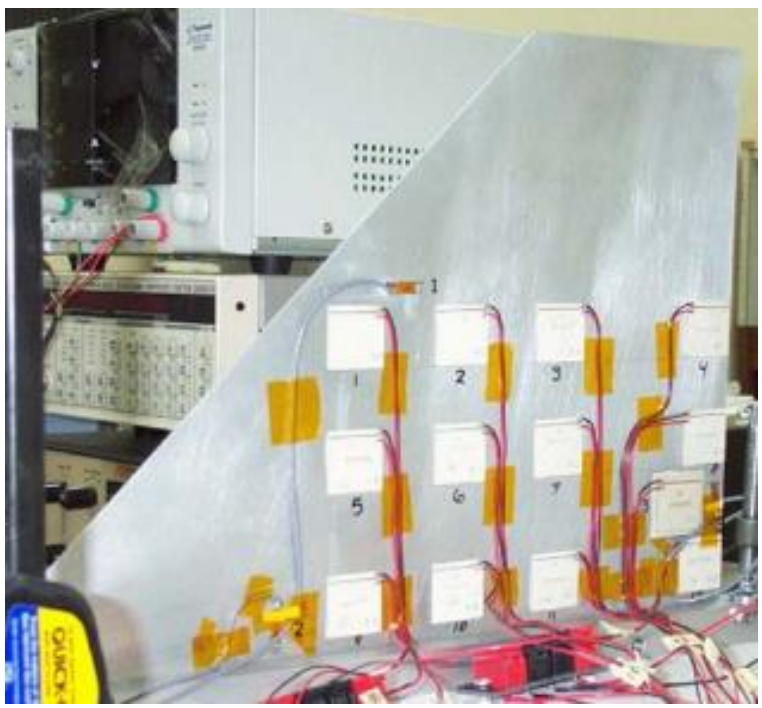

Figure 1.9 Experimental Construction of a Smart Fin Controlled by Piezoelectric Plates [14]

II. Methodology

2.1 Descriptions of the Subject of Study

Before determining the subject of the present research, a smart fin morphed by plates composed of piezoelectric materials was introduced. However, the pitching moment acted on the morphing airfoil under the flight speed of Mach 0.6 is greater than that of all-moving airfoil, as shown in Table 2.1. Thus, prior to the further study of the morphing smart fin, all-moving smart fin is considered in the present thesis. The smart fin studied in the present thesis is shown in Figure 2.1, represented as a left-hand side wing. The root of the smart fin is hidden in Figure 2.1, and the airfoil shape of the root is NACA 0015. The tip of the smart fin has geometry of NACA 0012, and the airfoil shell of the smart fin represents the tapered wing shape. The projected feature and some components are displayed in Figure 2.2 for clear comprehension [15]. The smart fin adjusts the flight attitudes and flight path by manipulating its pitch angle. The airfoil shell of the smart fin rotates on the axis of the shaft, by receiving moments generated by the actuator composed of piezoelectric material. The actuator denominated as 'PZT actuator' in the present thesis, and consists of five independent layers as shown in Figure 2.3. Three PI film layers hold and cover the two different plates, a carbon epoxy plate and a 3203HD plate, respectively. The layers are named after the materials, and the material properties are displayed in Table 2.2. The stress form of the piezoelectric matrix is introduced for better understandings about deformation of piezoelectric

material due to voltage. The strain form of piezoelectric material can be expressed in a matrix form in Equations (2.1) and (2.2), where ε is strain tensor, c is elasticity matrix, d is the component of the piezoelectric tensor, E is the electric field vector, σ is the stress tensor, P is the electric polarization vector, ϵ_0 is the permittivity of free space, and χ are the components of the electric susceptibility tensor [15].

$$\varepsilon = d^T E + c^{-1}\sigma \tag{2.1}$$

$$\mathrm{P} = \epsilon_0 \chi E + d\sigma \tag{2.2}$$

Multiplying Equation (2.1) by c, Equation (2.3) can be obtained.

$$c\varepsilon = cd^T E + \sigma \tag{2.3}$$

And Equation (2.3) can be solved for the stress matrix σ as expressed in Equation (2.4), where $e = cd^T$.

$$\sigma = c\varepsilon - cd^T E = c\varepsilon - eE \tag{2.4}$$

From Equation (2.2), Equation (2.5) can be obtained where ϵ^σ is the permittivity at constant stress, and D is the electric displacement vector. And then Equation (2.6) is obtained, where $\epsilon^\varepsilon = \epsilon^\sigma - de$, and this is the permittivity at constant strain.

$$\mathrm{D} = \mathrm{P} + \epsilon_0 E = \epsilon_0 \chi E + d\sigma + \epsilon_0 E = (\epsilon^\sigma - de)E + dc\varepsilon \tag{2.5}$$

$$\mathrm{D} = \epsilon^\varepsilon E + e^T \varepsilon \tag{2.6}$$

Then the piezoelectric stress matrix can be expressed by Equation (2.7).

$$e = cd^T = \begin{bmatrix} c_{11} & c_{12} & c_{13} & 0 & 0 & 0 \\ c_{12} & c_{11} & c_{13} & 0 & 0 & 0 \\ c_{13} & c_{13} & c_{33} & 0 & 0 & 0 \\ 0 & 0 & 0 & c_{44} & 0 & 0 \\ 0 & 0 & 0 & 0 & c_{44} & 0 \\ 0 & 0 & 0 & 0 & 0 & 2(c_{11}-c_{12}) \end{bmatrix} \begin{bmatrix} 0 & 0 & d_{31} \\ 0 & 0 & d_{31} \\ 0 & 0 & d_{33} \\ 0 & d_{15} & 0 \\ d_{15} & 0 & 0 \\ 0 & 0 & 0 \end{bmatrix}$$

$$= \begin{bmatrix} 0 & 0 & c_{11}d_{31}+c_{12}d_{31}+c_{13}d_{33} \\ 0 & 0 & c_{12}d_{31}+c_{11}d_{31}+c_{13}d_{33} \\ 0 & 0 & c_{13}d_{31}+c_{13}d_{31}+c_{33}d_{33} \\ 0 & c_{44}d_{15} & 0 \\ c_{44}d_{15} & 0 & 0 \\ 0 & 0 & 0 \end{bmatrix} \tag{2.7}$$

The strain, produced from the electric field, generates pitching moment with the moment arm, the distance from the shaft and the center of support part.

.

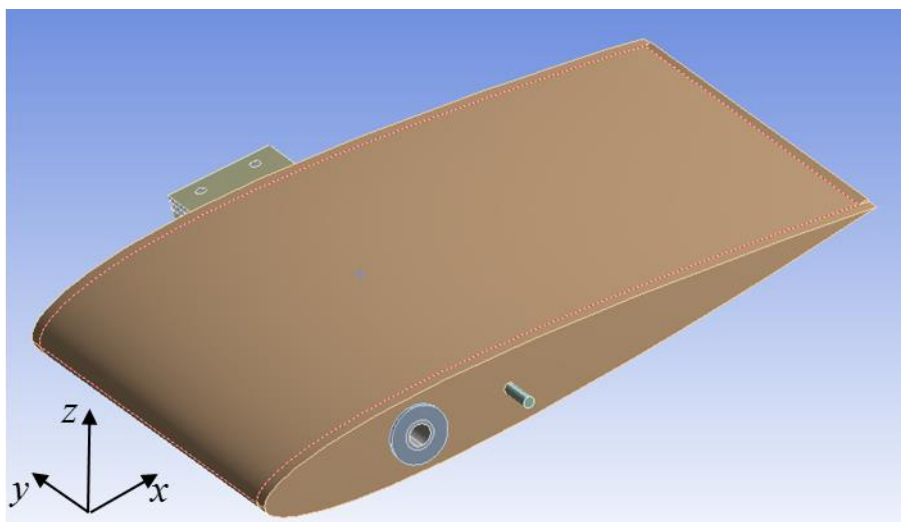

Figure 2.1 Subject of Study: Smart Fin

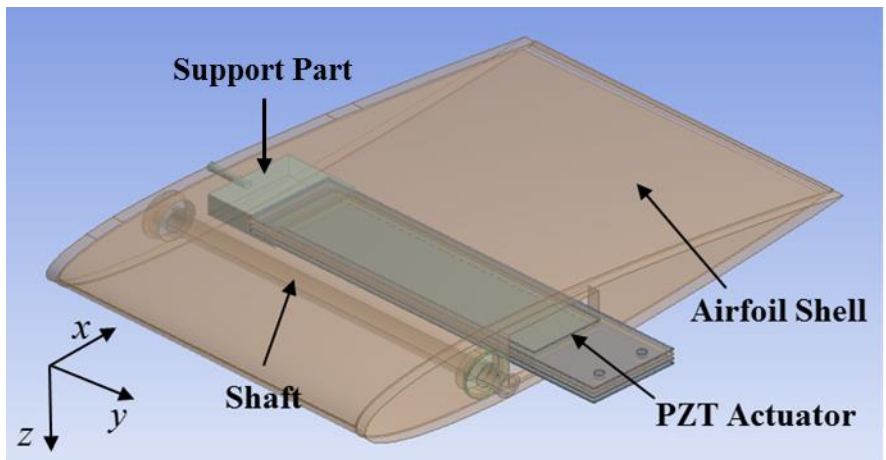

Figure 2.2 Projection of the Smart Fin and Denominations [15]

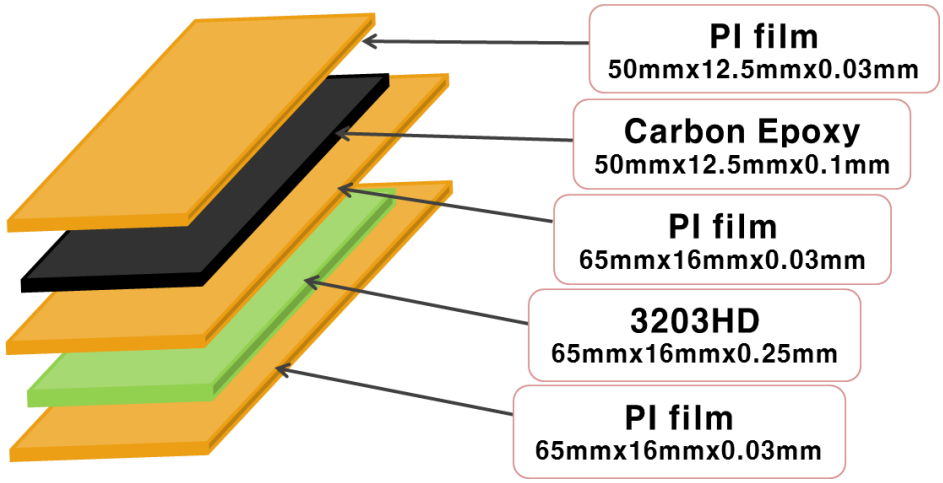

Figure 2.3 Construction and Dimension of PZT Actuator

Table 2.1 Pitching Moment of the Smart Fin with Angle of Attack of 10° in the Airflow of Mach 0.5

Pitching Moment (N · m/m)	Morphing Smart Fin	All-moving Smart Fin
Inviscid Flow	40.0	14.8
Turbulent Flow	32.7	11.2

Table 2.2 Material Properties of the PZT Actuator

Material Property	PI film	Carbon Epoxy	3203HD
Young's Modulus, E_1 (GPa)	3.0	66.42	62.0
E_2 (GPa)	-	-	62.0
E_3 (GPa)	-	-	49.0
Shear Modulus (GPa)	1.12	4.35	23.664
Poisson's ratio	1420.0	1510.0	7870.0
Piezoelectric strain constant			
$d_{31}(10^{-12}/v)$	-	-	-320
$d_{32}(10^{-12}/v)$	-	-	-320
$d_{33}(10^{-12}/v)$	-	-	650

2.2 Structural Analysis of the Smart Fin

To verify the static actuation correlation, the static structural analysis of the smart fin is performed by using ANSYS, and the result is compared with that obtained from experiments. The fundamental structural analysis is modal analysis. The results from the modal analysis, natural frequencies and mode shapes, are used to the further analysis required to be performed in the present thesis. The modal analysis of the smart fin is calculated by using MSC.NASTRAN. MSC.NASTRAN is a commercial calculating program of structural analysis, which combines modal analysis tool named as SOL103. MSC.NASTRAN uses application of finite element method to structural models, and the program also offers graphical user interface (GUI) through MSC.PATRAN program. In MSC.PATRAN, users can create structural model and meshes for finite elements and apply the material properties and boundary conditions. For the modal analysis of the smart fin, three dimensional finite element method is applied. The detailed processes and the results of modal analysis by using MSC.NASTRN and PATRAN are explained in Section 3.

2.3 Aeroelastic Analysis of the Smart Fin

Based on the structural analysis, the aeroelastic stability is performed with the flight condition of Mach number 0.6 for cruising. For flight in the desirable condition, the

smart fin must be structurally and aeroelastically stable. Flutter analysis based on the modal analysis of the smart fin is performed and ZAERO is used. For verification of the aerodynamics of ZAERO, ANSYS is introduced as the subject of comparison. ZAERO is an aeroelastic commercial tool, developed by Chen [16] in ZONA Technology, Inc. Chen established a new flutter solution technique called g-method, in addition to the p and p-k method [17]. ZAERO calculates the aerodynamics and aeroelastic characteristics, receiving the information of modal characteristics, the natural frequencies and mode shapes from MSC.NASTRAN. ZAERO uses panel methods, for example ZONA6 for subsonic flight, ZONA7 for supersonic flight, etc. The panel methods used in ZAERO is more developed method than doublet lattice method (DLM), by adopting more higher-order paneling scheme. Additionally, unsteadiness of flow is considered in the panel methods, by solving the flutter matrix equation in the reduced frequency domain, assuming simple harmonic oscillations. ZAERO offers the v-g plots, which represents the damping coefficient versus the flight speed, and the v-f plots, which also represents the frequency versus the flight speed, offering the flutter speeds, too. The v-g and v-f plots imply the degree of freedom of the flutter, and the oscillating frequency as well as the flutter speed. The two plots can be obtained from the flutter analysis in the frequency domain. ZAERO also can offer the flutter solution in time domain by using rational function approximation (RFA) techniques. RFA method can generate unintended error to the solution because it makes approximated matrices in the process of the flutter solution. Thus, the results from

flutter solution in time domain must be compared with those in frequency domain, which are supposed to be an exact solution. The detailed RFA techniques will be explained in section 2.4.

2.4 Aeroservoelastic Modeling of Smart Fin Control System

Complete aeroservoelastic closed-loop of the smart fin is constructed prior to the further aeroservoelastic analysis. The aeroservoelastic closed-loop conceptual block diagram for the smart fin control system is depicted in Figure 2.4, which is single-input-single-output (SISO) system. The final target required to be observed, is the pitch angle of the smart fin represented as the output, and the intended pitch angle is the input. The box named as 'PZT Actuator', and the very next box means aeroelasticity of the smart fin. Also, without a controller and gain, the system is called open-loop aeroservoelastic system of the smart fin in this paper. After the modal analysis of the smart fin, aeroelastic stability analysis is performed while the aerodynamics of the smart fin is calculated. And then the aeroservoelastic analysis with controller is performed in time domain to observe the structural time responses.

2.5 Theoretical Process of the Aeroservoelastic Analysis by State-Space Approach

Before the aeroservoelastic analysis by state-space form, equation of motion of aeroelastic system must be set in order to be coupled with control system. The following Equation (2.3) is the general equation of motion of aeroelastic system in the modal coordinates [16],

$$[M_{hh}]\{\ddot{\xi}\}+[C_{hh}]\{\dot{\xi}\}+[\mathrm{K}_{hh}]\{\xi\}+[M_{hc}]\{\ddot{\delta}\}=\mathrm{q}_{\infty}[Q_{hh}(\mathrm{ik})]\{\xi\}+\mathrm{q}_{\infty}[Q_{hc}(\mathrm{ik})]\{\delta\} \tag{2.8}$$

where $[M_{hh}]$, $[C_{hh}]$, $[K_{hh}]$ are the generalized mass, damping, and stiffness respectively, and $\{\xi\}$, $\{\delta\}$ are the generalized coordinates and control surface deflections, respectively. In the right hand side of Equation (2.8) is about the aerodynamic forces due to the structural deflections and control surface deflections where q_{∞} is the dynamic pressure $[Q(ik)]$ is the generalized aerodynamic force (GAF) matrices. In forming the state-space equations of the aeroelastic system from the equation of motion, the frequency domain GAF matrices need to be converted in the Laplace domain. After that, the Laplace domain unsteady aerodynamics have to be in a rational function in order that the GAF matrices can be integrated in the time domain state-space equations of the aeroelastic system. This progress is so-called rational function approximation (RFA) in the field of aeroelasticity. The general expression of the RFA is set up in Equation (2.9) [16],

$$[\tilde{Q}(s)]=[A_0]+\frac{L}{V}[A_1]s+\frac{L^2}{V^2}[A_2]s^2+[D]\left[s[I]-\frac{V}{L}[R]\right]^{-1}[E]s \tag{2.9}$$

where $[A_0]$, $[A_1]$ and $[A_2]$ are the aerodynamic stiffness, damping and apparent mass of the unsteady aerodynamics, respectively. Important thing in Equation (2.9) is $[R]$ matrix, defined as the aerodynamic lag states to model the aerodynamic lag effects due to the unsteady flow. The size of the lag states matrix $[R]$ is different from approximation methods. There have been two represent approximation methods of RFA, proposed by Roger [18] and Karpel [19]. The first one is Roger's method [18], which makes the size of the matrices of the state-space equations of the aeroelastic system relatively become larger than those of the second method called minimum state method, established by Karpel [19]. The lag states matrix $[R]$ from the Roger's method is represented in the following Equation (2.10) [16].

$$[D] = \left[[I]_{hh}, [I]_{hh}, ... \right]_{N_h \times N_{lag}}$$

$$[R] = \begin{bmatrix} \begin{bmatrix} \ddots & & \\ & R_i & \\ & & \ddots \end{bmatrix}_1 & & & \\ & \begin{bmatrix} \ddots & & \\ & R_i & \\ & & \ddots \end{bmatrix}_2 & & \\ & & \ddots & \\ & & & \begin{bmatrix} \ddots & & \\ & R_i & \\ & & \ddots \end{bmatrix}_{N_h} \end{bmatrix}_{(N_h \times N_{lag}) \times (N_h \times N_{lag})}$$

(2.10)

$$[R] = \begin{bmatrix} R_1 & & & \\ & R_2 & & \\ & & \ddots & \\ & & & R_{N_{lag}} \end{bmatrix}_{N_h \times N_{lag}} \tag{2.11}$$

N_h denoted in Equation (2.10) means the number of modes, and R_i is the $i-th$ aerodynamic lag state. The size of lag state matrix $[R]$ can be extremely large if the number of structural modes in the aeroelastic system is large. Another RFA method, the minimum state method prevents the size of the lag state matrix $[R]$ from being extremely large. Unlike the Roger's method, the matrix $[R]$ has only the lag states in

the diagonal term as described in Equation (2.11) [16], so the size of the overall state-space equation of the aeroelastic system can reduce. It is evident for the number of the aerodynamic lag states to be larger than that of Roger's method to satisfy high accuracy of the RFA. The results using RFA are typically more accurate for larger number of lag states, however, a large number of aerodynamic lag states can induce fatal error by giving an over-fitted RFA. The large number of aerodynamic lag states also results in the large size of the state-space equation of the aeroelastic system so gives difficulty to the control designer when using control law [16]. The appropriate number of aerodynamic lag states must be determined through a trial-and-error by comparing the flutter results with those obtained from frequency domain.

Back to the equation of motion of the aeroelastic system, it is ready to facilitate the state-space formulation with the RFA results. The resulting state-space equation of the aeroelastic system is as following Equation (2.12), and also some matrices of that are displayed in Equations (2.13) and (2.14) [16].

$$\begin{aligned} \{\dot{X}_{ae}\} &= [A_{ae}]\{X_{ae}\} + [B_{ae}]\{U_{ae}\} \\ [y_{ae}] &= [C_{ae}]\{X_{ae}\} + [D_{ae}]\{U_{ae}\} \end{aligned} \tag{2.12}$$

$$[A_{ae}]=\begin{bmatrix} [0] & [I] & [0] \\ -[\bar{M}]^{-1}[[K_{hh}]-q_{\infty}[A_{hh_0}] & -[\bar{M}]^{-1}[[C_{hh}]-q_{\infty}\frac{L}{V}[A_{hh_1}] & q_{\infty}[\bar{M}]^{-1}[D] \\ [0] & [E_h] & \frac{V}{L}[R] \end{bmatrix} \tag{2.13}$$

$$[B_{ae}]=\begin{bmatrix} [0] & [0] & [0] \\ q_{\infty}[\bar{M}]^{-1}[A_{hc_0}] & q_{\infty}\frac{L}{V}[\bar{M}]^{-1}[A_{hc_1}] & -[\bar{M}]^{-1}\left[[M_{hc}]-\frac{q_{\infty}L^2}{V^2}[A_{hc_2}]\right] \\ [0] & [E_c] & [0] \end{bmatrix} \tag{2.14}$$

The term $[R]$ in the Equation (2.13) represents the aerodynamic lag states, so the size of the matrix $[A_{ae}]$ depends on the number of the aerodynamic lag states.

Adding an actuator to the aeroelastic system, it is called an open-loop aeroservoelastic system in this thesis. The characteristic of the actuator can be expressed by a transfer function, and the transfer function can be transformed in the state-space form for the further aeroservoelastic analysis, in the time domain. The representative transfer function of the actuator in Equation (2.15) can be directly transformed to the state-space formulation in Equation (2.16) [16].

$$\Delta=\frac{a_0}{s^3+a_2s^2+a_1s+a_0}u_{act} \tag{2.15}$$

$$\{\dot{X}_{act}\} = \begin{bmatrix} 0 & 1 & 0 \\ 0 & 0 & 1 \\ -a_0 & -a_1 & -a_2 \end{bmatrix} \{X_{act}\} + \begin{Bmatrix} 0 \\ 0 \\ a_0 \end{Bmatrix} u_{act} \tag{2.16}$$

The state-space equation in Equation (2.16) can be integrated by combining with Equation (2.12), thus the aeroelastic system with an actuator can obtained as in Equation (2.17). This system is called 'plant' in this thesis.

$$\begin{aligned} \{\dot{X}_p\} &= [A_p]\{X_p\} + [B_p]\{U_p\} \\ \{y_p\} &= [C_p]\{X_p\} \end{aligned} \tag{2.17}$$

The aeroservoelastic closed-loop system introduced in Section 2.4 and in Figure 2.4, is the system adding a controller into the 'plant' for the feedback control. The characteristic of the controller, like the actuator, can be expressed by a transfer function and state-space formulation as displayed in Equations (2.18) and (2.19), respectively.

$$y_c(s) = \frac{b_0 s^n + b_1 s^{n-1} + \cdots + b_n}{s^n + a_1 s^{n-1} + \cdots + a_n} u_c(s) \tag{2.18}$$

$$\begin{aligned} \{\dot{X}_c\} &= [A_c]\{X_c\} + [B_c]\{U_c\} \\ \{y_c\} &= [C_c]\{X_c\} + [D_c]\{U_c\} \end{aligned} \tag{2.19}$$

Equation (2.19) can be also incorporated with the state-space equation of the 'plant', thus, Equation (2.20) can be finally facilitated, which is the state-space equation of the aeroservoelastic system expressed as the smart fin control system. The closed-loop

block diagram in Figure 2.4 is provided with a gain expressed in Equation (2.21). Within the gain parameters in Equation (2.21), only the G_{pc} is non-zero in this analysis.

$$\begin{aligned}\{\dot{X}_v\} &= [A_v]\{X_v\} + [B_v]\{U_v\} \\ \{y_v\} &= [C_v]\{X_v\} + [D_v]\{U_v\}\end{aligned} \tag{2.20}$$

$$\{U_v\} = [G_v]\{y_v\} \Leftrightarrow \begin{Bmatrix} U_p \\ U_c \end{Bmatrix} = \begin{bmatrix} G_{pp} & G_{pc} \\ G_{cp} & G_{cc} \end{bmatrix} \begin{Bmatrix} y_p \\ y_c \end{Bmatrix} \tag{2.21}$$

The state-space equations of the 'plant' provides the time responses and Bode plots, root locus for the stability analysis. Furthermore, for the 'plant', adequate controller can be designed to satisfy the flight requirements about the smart fin control system studied in this thesis.

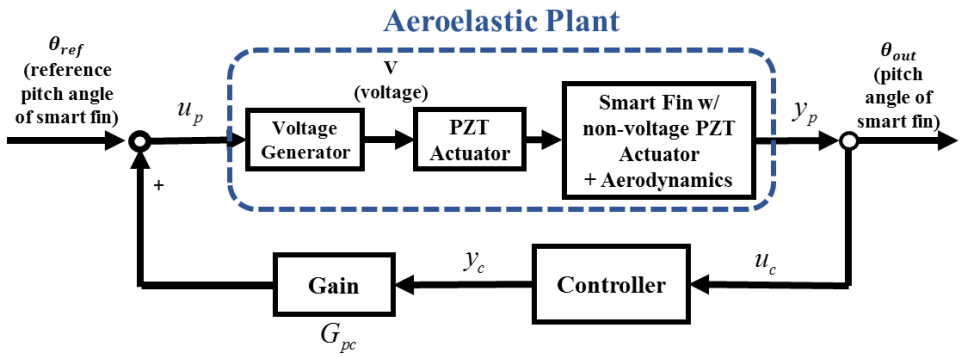

Figure 2.4 Aeroservoelastic Closed-loop Conceptual Block Diagram of the Smart Fin Control System

III. Results

3.1 Structural Analysis of the Smart Fin

3.1.1 Static Structural Analysis

For the structural model, introduced in Figures 2.1 and 2.2, static structural analysis and experiment are performed. For the 450 V applied, the pitch angles from ANSYS and an experiment, are shown in Table 3.1 under a condition of no flow around the smart fin. Additionally, the equivalent moment to the applied voltage is calculated based on theory of smart material. Then, the pitch deflection versus the equivalent moment, is also predicted by ANSYS [20]. The three pitch deflection results are presented in Table 3.1 at the same time. According to Table 3.1, the pitch deflection results assure the correlation between the analysis and the experiment.

3.1.2 Structural Modal Analysis

With the same structural model, material properties, and boundary conditions [15], the structural modal analysis is performed by using MSC.NASTRAN. MSC.NASTRAN is a well-known commercial structural computing program. In this section, the results structural analysis, especially about the modal analysis of the smart fin are displayed. First, the structural model of the smart fin made in CATIA, the step file is imported to the MSC.PATRAN, which is a pre/post processor of various MSC

software programs in addition to MSC.NASTRAN. Material properties of the smart fin are set in the next stage. The main properties of the PZT actuator are already explained in Table 2.1 and more, the airfoil shell is composed of 'polycarbonate', which is an isotropic plastic material. The density, Young's modulus, and Poisson's ratio of 'polycarbonate' are 1210 kg/m^3, 2.2 GPa, and 0.37, respectively. The material property of the other parts of the smart fin is aluminum. After assigning materials, meshes are made for applying finite element method (FEM) as depicted in Figure 3.1. The meshes form the total number of nodes, reaching approximately 160 thousands. The last setting, the boundary conditions are same with those set from ANSYS, however, one of them is a little different. The support part and the airfoil shell indicated in Figure 2.2, are glued each other in MSC.NASTRAN because the contact condition in SOL103 for the modal analysis, is permitted only to set as 'glue' condition, not 'touch'. The shaft, also depicted in Figure 2.2, is constrained to be allowed to move in only pitch rotation, in that, the shaft has only one degree of freedom. The SOL 103 is used for the modal analysis of the smart fin and 10 structural modes are obtained. Figure 3.2 and Table 3.2 are the results of modal analysis. Throughout the natural mode shapes in Figure 3.2, there are some local modes, and the first mode is related to the pitch motion. Almost natural frequencies are around 1000 Hz, with the first natural frequency of 23 Hz, as shown in Table 3.2. If the 'touch' condition is applied to the boundary condition in MSC.NASTRAN, the natural frequencies will become smaller than the current results.

Table 3.1 Results of Static Structural Analysis Obtained from ANSYS and Experiment [20]

	ANSYS (Applied voltage)	ANSYS (Equivalent moment)	Experiment
Deflection in Pitch Angle	**3.45° (+3.92 %)**	**3.73° (+12.3%)**	**3.32°**

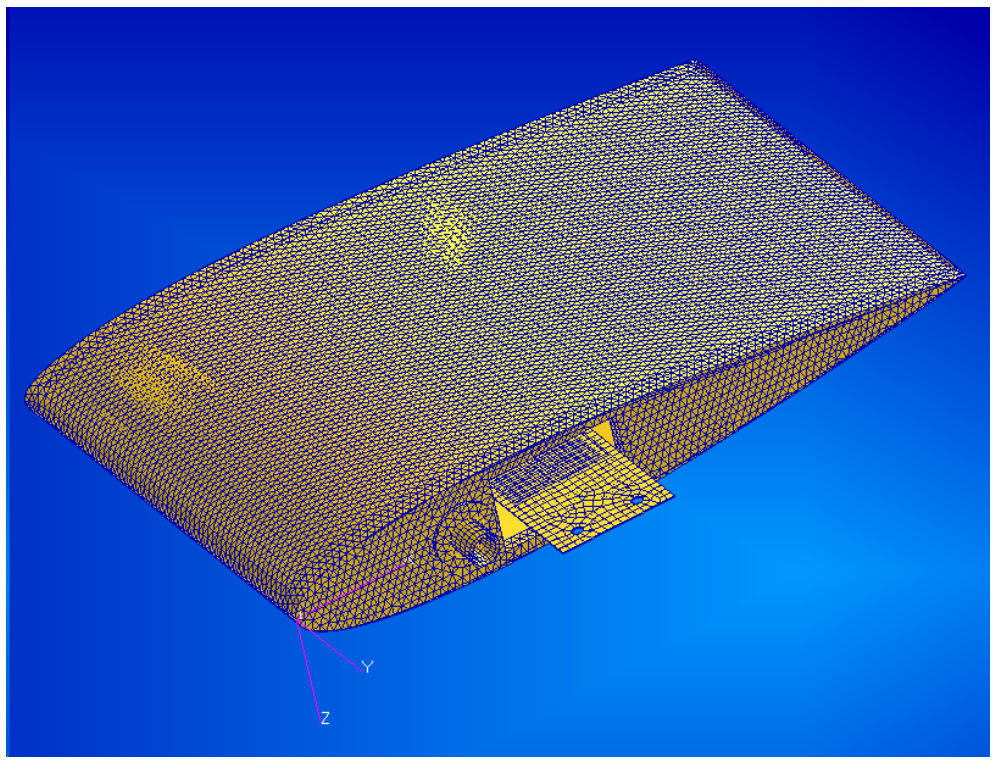

Figure 3.1 Finite Elements of Smart Fin Created in MSC.PATRAN

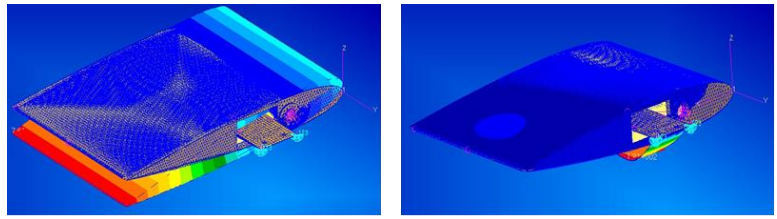

(a) 1st mode

(b) 2nd mode

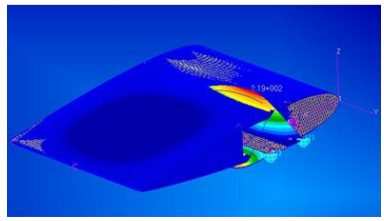

(c) 3rd mode

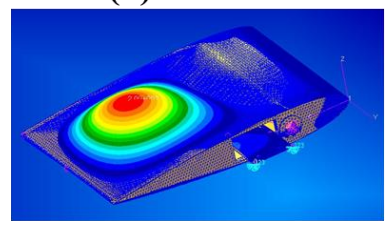

(d) 4th mode

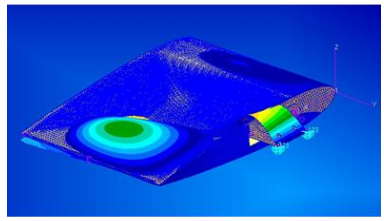

(e) 5th mode

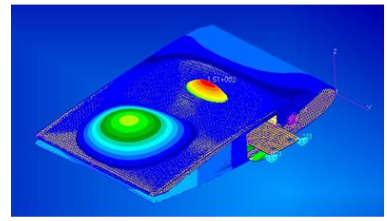

(f) 6th mode

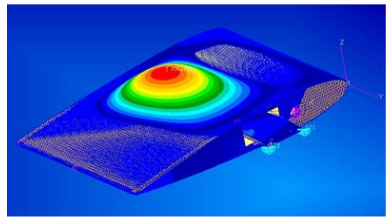

(g) 7th mode

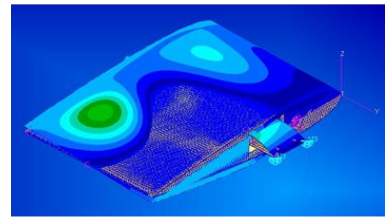

(h) 8th mode

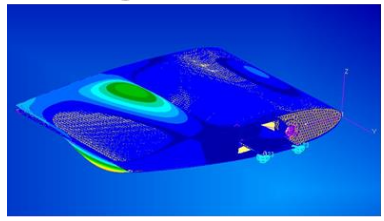

(i) 9th mode

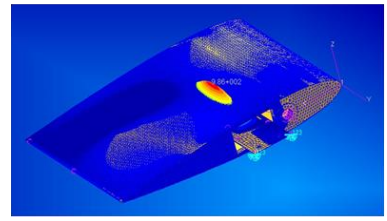

(j) 10th mode

Figure 3.2 Natural Mode Shapes of the Smart Fin

Table 3.2 Natural Frequencies of the Smart Fin

Natural Mode	Natural Frequency, Hz
1st mode	23.107
2nd mode	384.97
3rd mode	869.25
4th mode	951.21
5th mode	1075.3
6th mode	1191.5
7th mode	1218.5
8th mode	1417.1
9th mode	1563.9
10th mode	1611.0

3.2 Aeroelastic Stability Analysis of the Smart Fin

3.2.1 Aerodynamics of the Smart Fin Using ZAERO

For verification of the aerodynamics using ZAERO, the aerodynamic coefficients obtained from both ANSYS and ZAERO are compared with each other. Using TRIM module of ZAERO, the lift, drag, and pitching moment coefficients are obtained under the assumption of inviscid and incompressible flow. In both ANSYS and ZAERO, the structural model of the smart fin is a three-dimensional structure, and the airfoil has angle of attack of 4°. Table 3.3 shows the comparison of the two results regarding the aerodynamic coefficients.

3.2.2 Flutter Analysis of the Smart Fin Using ZAERO

For aeroelastic stability, flutter analysis is performed by using ZAERO. ZAERO has a special technique to solve flutter problem, called g-method developed by Chen [17]. The present flutter analysis is obtained by applying the g-method. For the desirable flight speed of Mach number 0.6, ZONA6 lifting surface method is used to compute the aerodynamics. ZONA6 is apt to compute the aerodynamics in the subsonic flight condition, and this method is very similar to the doublet lattice method (DLM), one of the panel method. However, ZONA6 adopts a higher-order paneling scheme than DLM so ZONA6 has advantage in robustness of the unsteady lifting surface methods [21]. It

is also appeared that ZONA6 is more accurate than DLM even for high reduced frequency conditions [16]. In ZAERO, importing the results of modal analysis of smart fin from MSC.NASTRN, interaction between structure and air flow are computed by splining the aerodynamic panels with structural grids. The flutter analysis of the smart fin is performed in the frequency. In the present flutter solution, the flight conditions are as follows: sea level (air density, 1.228 kg/m^3), reference Mach number 0.6, while considered reduced frequency region from 0 to 0.95. ZAERO offers the flutter speeds with oscillational frequencies, and they are depicted in Table 3.4. The flutter solutions using non-matched flutter solution show that the flutter speed of the smart fin is about 282 m/s, approximately equivalent to Mach number 0.827. The flutter results imply that the smart fin slightly has aeroelastically unstable potential in the flight condition of Mach number 0.6. ZAERO also offers the v-g and v-f plots, and they are plotted in Figure 3.3 and Figure 3.4, respectively.

Table 3.3 Aerodynamic Coefficients of the Smart Fin Obtained from ANSYS and ZAERO

Aerodynamic Coefficients	ANSYS	ZAERO
Lift coefficient	0.10687	0.26409
Drag coefficient	0.01027	0.00922
Pitching moment coefficient	0.01545	0.01830

Table 3.4 Flutter Solution of the Smart Fin from ZAERO

Flutter Mode	Flight Speed (m/s) at G=0	Frequency (Hz) at G=0
1st mode	282.2	0.0
3rd mode	765.5	455.2
4th mode	591.9	1113.1
7th mode	599.1	1604.5
8th mode	534.0	0.0

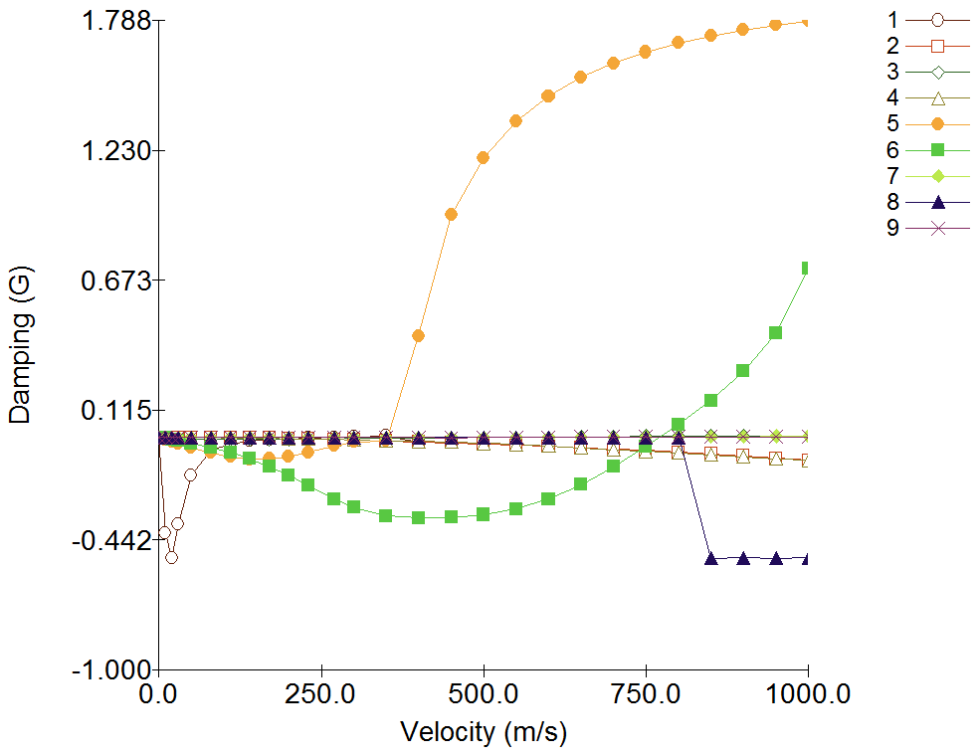

Figure 3.3 Damping versus Velocity from 1 to 9 Natural Modes of Flutter Solution Using G-method

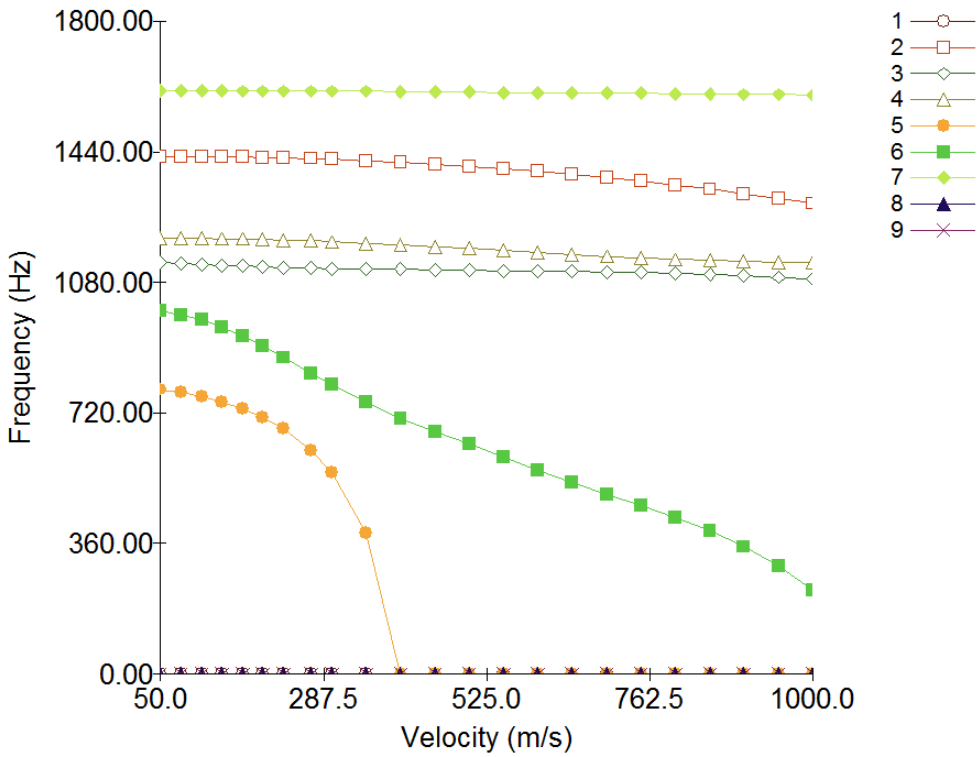

Figure 3.4 Frequency versus Velocity from 1 to 9 Natural Modes of Flutter Solution Using G-method

3.3 Open-Loop Aeroservoelastic Analysis of Smart Fin

Open-loop aeroservoelastic analysis is performed both in time domain and frequency domain by using ZAERO. The time domain analysis is for the purpose of obtaining the state-space equations containing the characteristics of PZT actuator as well as the structures and aerodynamics of the smart fin, such as Equation (2.17) in Section 2.5. The state-space equations of the open-loop aeroservoelastic system of the smart fin correspond to the 'AE Plant' box in Figure 3.5, which is from the analytical system of ZAERO [15]. The matrices in the state-space equation of the aeroservoelastic system can be used to simulate the structural responses for the given flight conditions. The frequency domain analysis is for the purpose of comparing the results from the time domain with it, while it is considered as the exact solution. It is because approximation method is used in time domain, called rational function approximation (RFA), which is already referred in Section 2.5. RFA can introduce error in the system due to approximation so it is necessary to compare the results from the time and frequency domain each other. The frequency domain analysis can also offer Bode plot and root locus, which show the stability margin and the characteristics of the open-loop aeroservoelastic system of the smart fin. The results from the frequency domain analysis are analyzed to design a controller to be added to the closed-loop aeroservoelastic system for the purpose of the control of the flight attitudes, the pitch angle of the smart fin.

3.3.1 Open-Loop Aeroservoelastic Analysis in the Frequency Domain

The frequency domain analysis, considered as the exact solution method, is performed by using ASE module of ZAERO. Like the flutter solution, the modal analysis of the smart fin is imported to the ZAERO input and mgg file also imported. Mgg file is about the mass information of the smart fin and this also obtained from MSC.NASTRAN by coding the DMAP in the MSC.NASTRAN input file. The flight conditions are the same with the flutter solution, explained in Section 3.2. The open-loop aeroservoelastic system is also quoted as plant. The plant of the smart fin contains the structures, aerodynamics, and the PZT actuator. The flutter results of the plant are also obtained in this frequency domain. Generally, the flutter results from the open-loop aeroservoelastic analysis are very similar with those from flutter solution, represented in Table 3.4. In this thesis, 'open-loop' means that the behavior of the plant is simulated without control. Table 3.5 shows the flutter speeds from the open-loop aeroservoelastic analysis, and the results are very similar with the results in Table 3.4. The Bode plots of the plant are depicted versus each flight speeds, 10 m/s, 20 m/s, 30 m/s, and 200 m/s (equivalent to approximately Mach 0.6) in Figure 3.6.

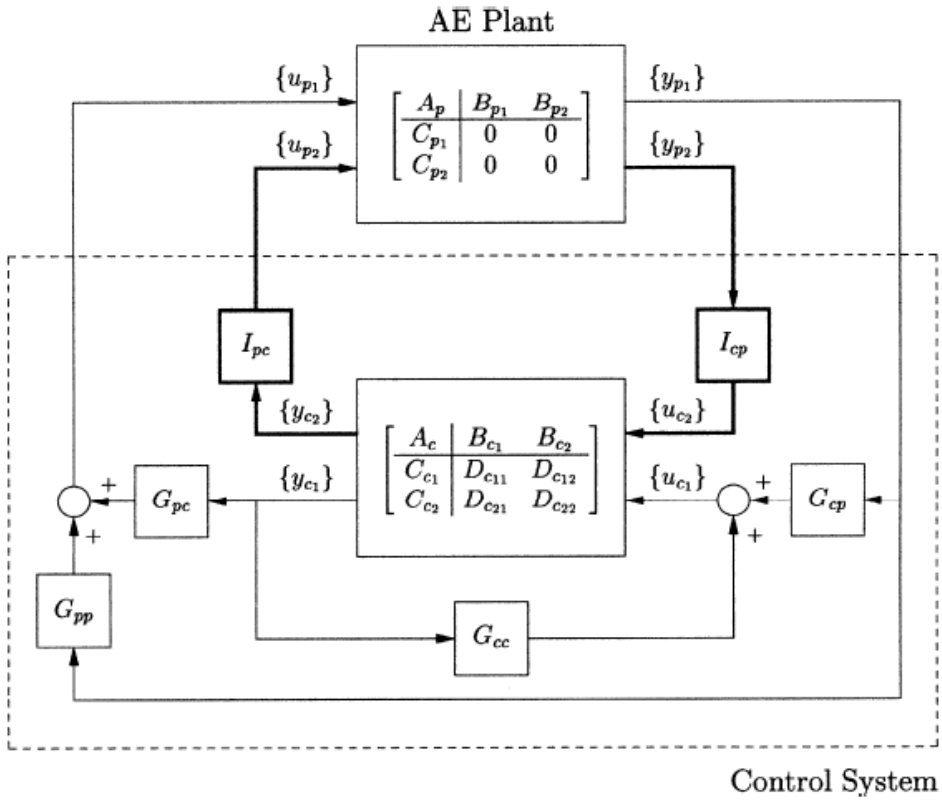

Figure 3.5 Aeroservoelastic Interconnection Model and the Matrices of State-Space Equations Applied in ZAERO

Table 3.5 Flutter Solution of the Smart Fin from Open-Loop Aeroservoelastic Frequency Domain Analysis

Flutter Mode	Flight Speed at G=0	Frequency at G=0
1st mode	282.2	0.0
3rd mode	765.5	455.2
4th mode	591.9	1113.1
7th mode	599.1	1604.5
8th mode	534.0	0.0

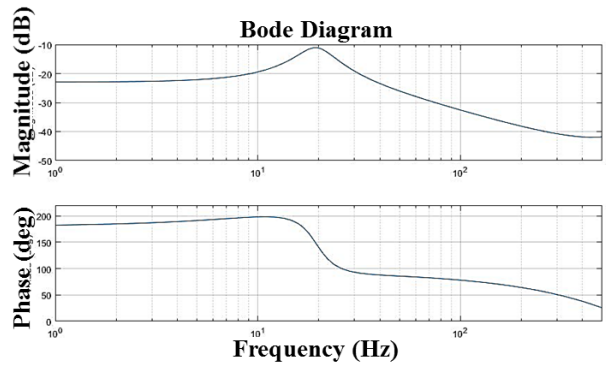

(a) Flight speed: 10 m/s

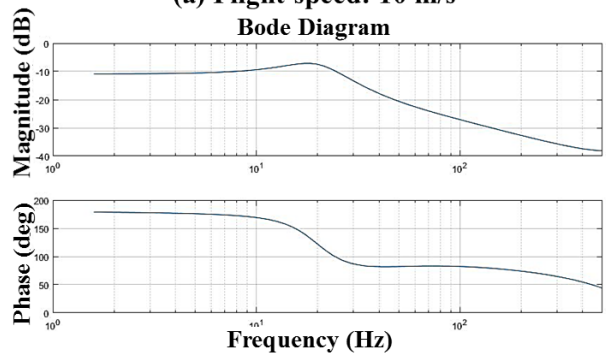

(b) Flight speed: 20 m/s

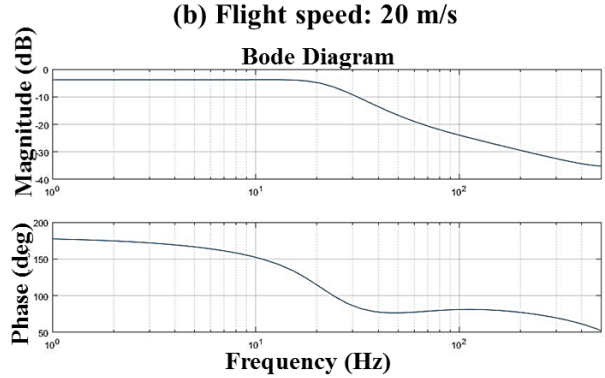

(c) Flight speed: 30 m/s

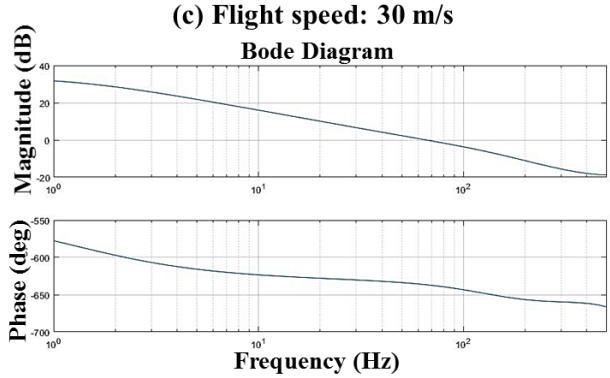

(d) Flight speed: 200 m/s

Figure 3.6 Bode Plots of the Plant at Each Flight Speed

3.3.2 Open-Loop Aeroservoelastic Analysis in Time Domain

In the open-loop aeroservoelastic analysis in time domain, ZAERO offers the matrices of the state-space equations for further the simulation of the structural responses. In this process, RFA is used, and the flutter solutions from time domain analysis are compared and verified for reducing the error, which can be introduced in the process of approximation of rational functions. The parameter, which can adjust the RFA method, is only the number of aerodynamic lag states. This number is determined as the best appropriate number to produce similar flutter results from time domain with those from frequency domain. The most adequate number for the aerodynamic lag states is two in this analysis, and the flutter results from the open-loop aeroservoelastic time domain analysis are presented in Table 3.6. According to Tables 3.5 and 3.6, the flutter speed is predicted to be 282 m/s, and the flutter mode is the first natural mode. With this comparison, the open-loop aeroservoelastic time domain analysis using RFA is verified. In this analysis, the output parameter is at the point of the trailing edge in the semi-span, so y in Equation (2.17) represents the displacement of the position in the z-direction (the positive z-direction is towards the sky). The matrices of the state-space equation of the plant, are extracted and further compose the plant in MATLAB. Figure 3.7 presents the step responses of the plant under each flight speed, same as those in Figure 3.6. The step responses are found to be more stable as the flight speed increases, with decreasing the amplitude of oscillation. However, for the flight speed of 200 m/s, the response does not converge within 0.1 second, not satisfying the settling time

requirement of the smart fin. The plunge magnitudes also tend to be large as the flight speed increases.

Table 3.6 Flutter Solution of the Smart Fin from Open-Loop Aeroservoelastic Time Domain Analysis

Flutter Mode	Flight Speed at G=0	Frequency at G=0
1st mode	282.2	0.0
3rd mode	596.8	1112.8
5th mode	351.6	377.3
6th mode	771.0	451.1
7th mode	601.8	1604.5
9th mode	534.0	0.0

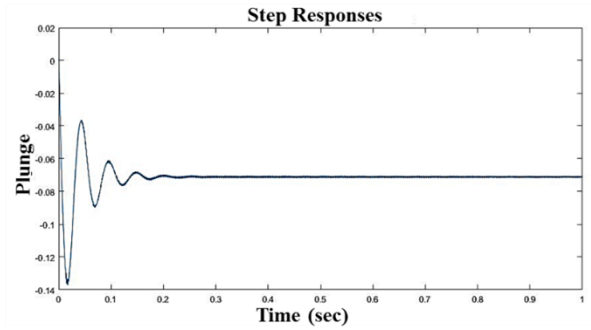

(a) Flight speed: 10 m/s

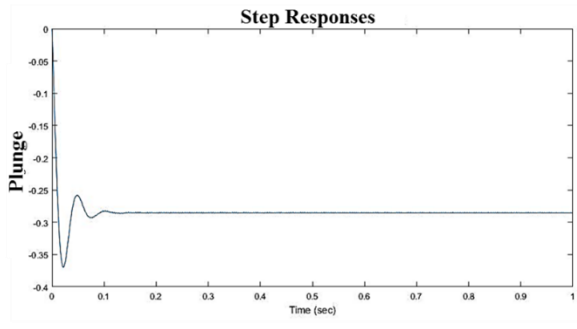

Time (sec)

(b) Flight speed: 20 m/s

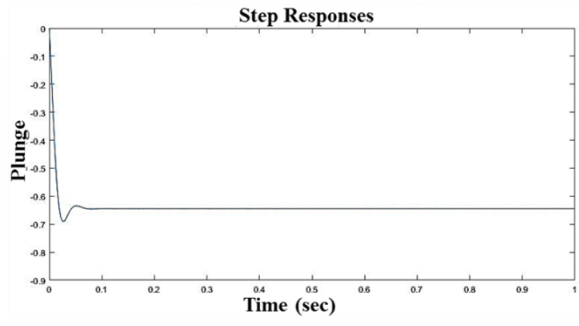

(c) Flight speed: 30 m/s

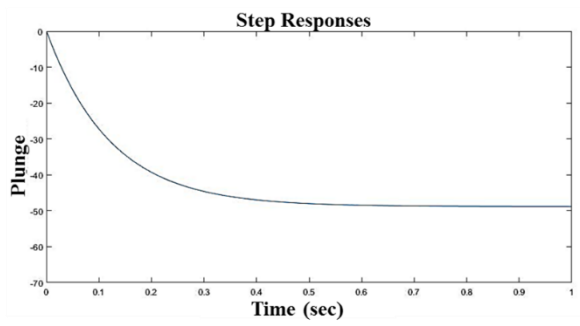

(d) Flight speed: 200 m/s

Figure 3.7 Step Responses of the Plant at Each Flight Speed

3.4 Closed-Loop Aeroservoelastic Analysis of Smart Fin

With the plant of the Section 3.3 from ZAERO, closed-loop control system of the smart fin is built in two programs. One of the programs is ZAERO, and this offers the new flutter results of the complete control system with controller. The other is MATLAB/Simulink, and this offers primarily the time simulation of the structural responses of the smart fin under a specific flight condition. The two approaches are explained in detail in the next sections.

3.4.1 Closed-Loop System Built by ZAERO

To set up the closed-loop control system in ZAERO, understanding of the aeroservoelastic interconnection model in Figure 3.5, is needed. The block diagram built in ZAERO, corresponds to Figure 2.4, and a controller is designed based on the classic control law. Referred to Bode plot of the plant in Figure 3.6, a transfer function of the controller is designed as shown in Equation (3.1).

$$Controller(s) = \frac{0.05598s + 6.88336}{s + 24.5924} \tag{3.1}$$

The transfer function is inserted to the SISOTF bulk data card of ASE module in ZAERO. The aeroservoelastic analysis is performed in frequency domain, and the new flutter speed is found to be 350 m/s, greater by about 24 % than that from open-loop aeroservoelastic analysis. At this time, the gain value, depicted in Figure 2.4, is 1.0, and as the gain is increased, the flutter speed of the closed-loop control system is also

increased. However, the saturation of the voltage input is not considered in this analysis using ZAERO. So MATLAB/Simulink is introduced as the complementary measure for the limitation of ZAERO in the next section.

3.4.2 Closed-Loop System Built by MATLAB/Simulink

Based on the plant of the smart fin obtained from the open-loop aeroservoelastic analysis using ZAERO, the closed-loop system of the smart fin control system is also established with PI controller under the flight condition of the aimed flight speed, 200 m/s, in MATLAB/Simulink as shown in Figure 3.8. The closed-loop control system is single-input and single-output (SISO) system, whose input and output is the pitch angle of the smart fin. The input of the pitch angle is transferred into 'Saturation' block box in Figure 3.8, because in reality the voltage input to the piezoelectric actuator is allowed within the limit value of $\pm$ 450 V. The equivalent pitch angle for the value of 450 V is 3.32° according to Table 3.1. Additionally, considering the aerodynamic force acting on the smart fin, the saturation limit of the input of the pitch angle is reduced to be $\pm$ 1.16°. The saturated input goes through 'PI Controller' and enters the 'Plant System' block box, which considers the characteristics of the structures of smart fin containing the piezoelectric actuator and the aerodynamics, and is finally fed back. The PI controller is explained in detail. To satisfy the requirements explained in section 2.1, especially the settling time condition, a PI controller is introduced and designed. According to Figure 3.7(d), after about 0.5 second, the plunge magnitude converges at the given flight

speed of 200 m/s, which is the desired cruise flight speed of the smart fin. However, one of the requirements of the smart fin is 1 degree of pitch angle at 10 Hz, in that, the smart fin must respond to the pilot input within 0.1 second. This condition is represented as the settling time in the present paper. To meet this requirement, PID tuner tool in MATLAB/Simulink is used. The PID tuner offers the parameters contained in PI controller, tuned based on the user's requirements. The default transfer function form of the PI controller is like equation (3.2), and the P, I, D, and N are obtained in the PID tuner tool.

$$P + I\frac{1}{s} + D\frac{N}{1 + N\frac{1}{s}} \tag{3.2}$$

The PID tuner tool also gives the parameters of performance and robustness of the control system as following factors: rise time, settling time, overshoot, peak, gain and phase margin, and the closed-loop stability. With the plant system in the flight condition of the flight speed, 200 m/s, the transfer function of the PI controller is set as displayed in Equation (3.3).

$$\mathrm{PID}(s) = -0.19437 - 5.8999\frac{1}{s} \tag{3.3}$$

The pilot input of the pitch angle is selected to the step input of 3 degrees and the corresponding output follows well the step input as shown in Figure 3.9. At the same time, the control performance and robustness are written in Table 3.8. The resulting

settling time meet the requirements of the smart fin, because it is lower than 0.1 second with flight speed of 200 m/s, approximately Mach number 0.6. Figure 3.10 shows the comparison between the open-loop system and closed-loop system with a controller of Equation (3.3).

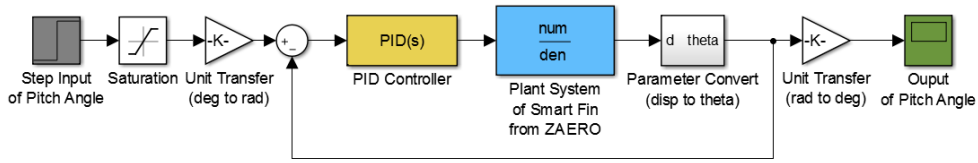

Figure 3.8 Closed-loop of Aeroservoelasic Smart Fin Control System Constituted in MATLAB/Simulink

Table 3.7 Tip Deflection of the Piezoelectric Actuator Corresponding to the Input Voltage

Input Voltage (V)	Deflection of PZT Actuator (mm)
100	4.167
200	8.167
300	11.833
400	17.5

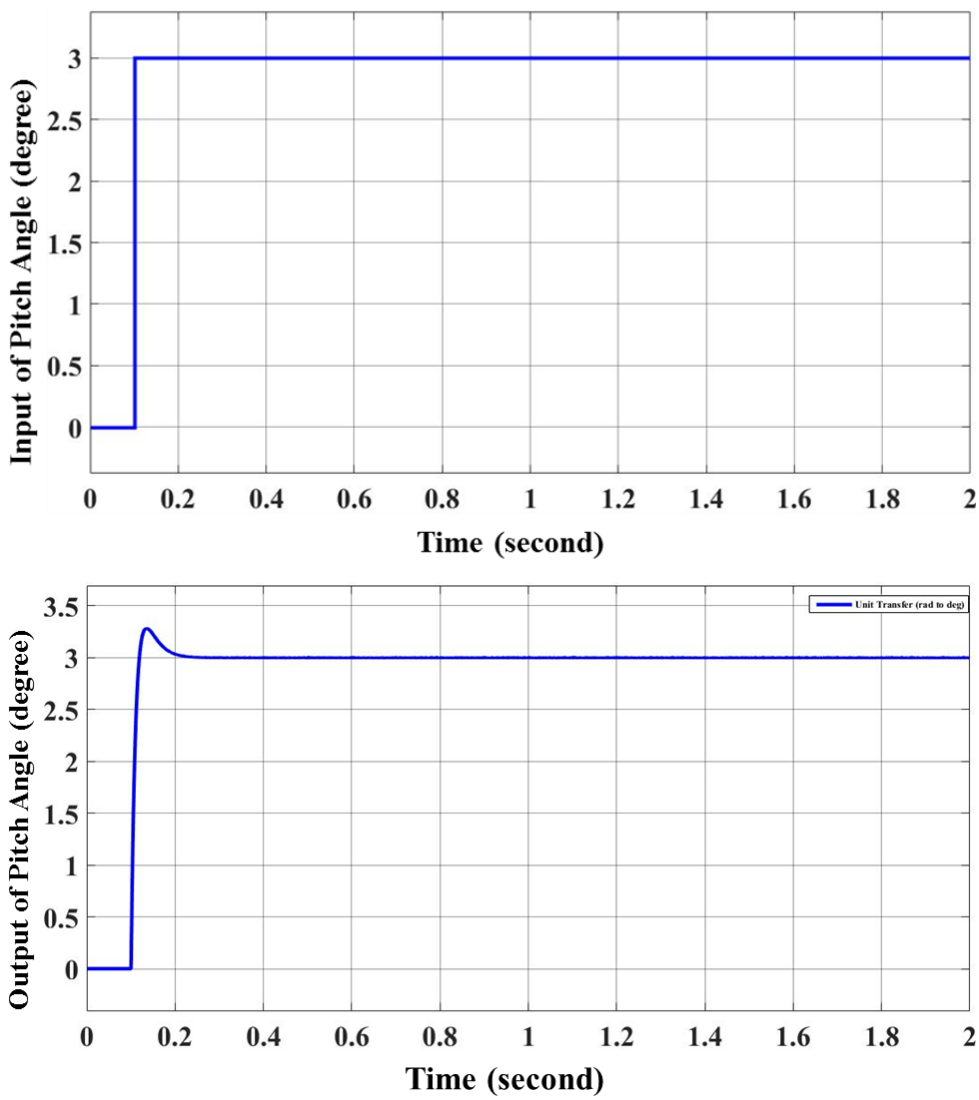

Figure 3.9 Step Input and Output of Pitch Angle of the Smart Fin from MATLAB/Simulink (Flight Speed: 200 m/s)

Table 3.8 Performance and Robustness of the Smart Fin Control System Compared to the Open-Loop System (Flight Speed: 200 m/s)

Performance Parameter	Open-Loop System	Closed-Loop System
Rise time	0.268 seconds	0.0144 seconds
Settling time (error ±1%)	0.56 seconds	0.0871 seconds
Overshoot	0.0%	9.12 %
Peak	1.0 (Reference 1.0)	1.09 (Reference 1.0)
Gain margin	4.29 dB @681 Hz	23.3 dB @681 Hz
Phase margin	83° @65.7 Hz	78° @18.8 Hz

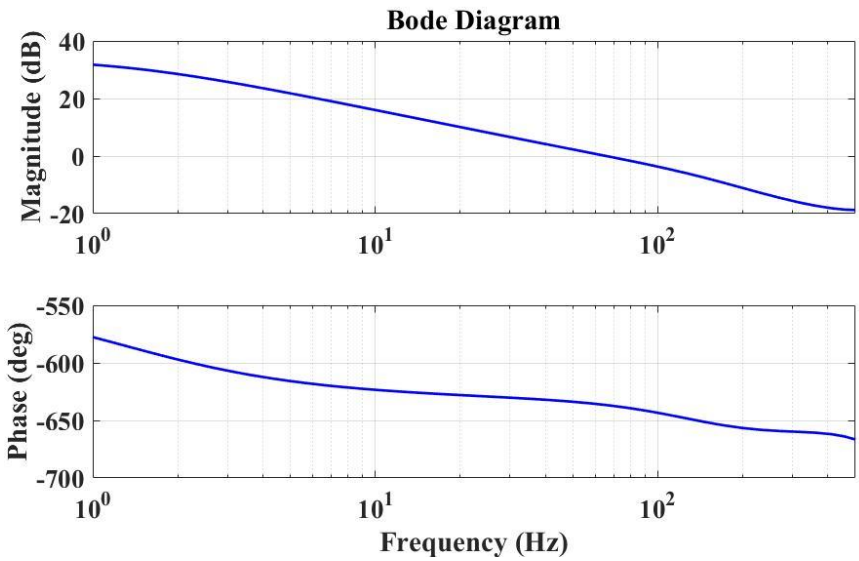

(b) Open-Loop System

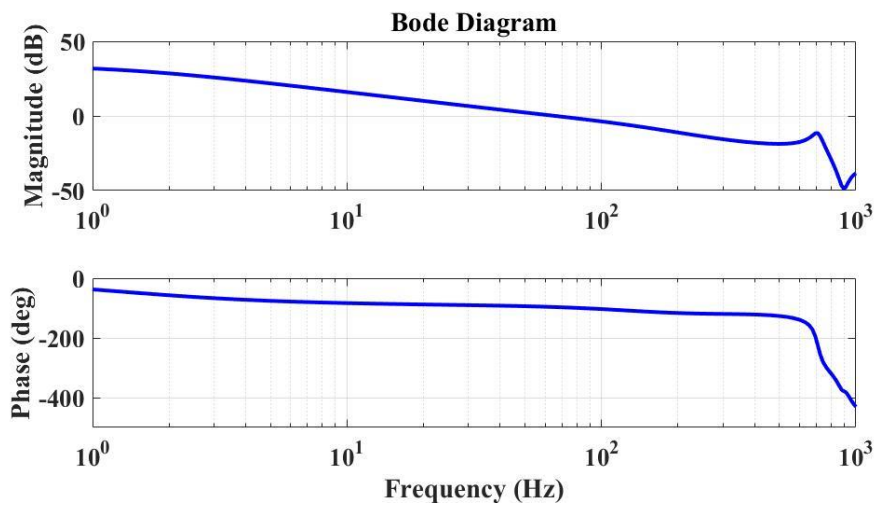

(a) Closed-Loop System

Figure 3.10 Bode Plots of both Open-Loop and Closed-Loop System of the Smart Fin Obtained from MATLAB/Simulink (Flight Speed: 200 m/s)

IV. Conclusions

By using MSC.NASTRAN and ZAERO, the modal analysis and the aeroelastic analysis are performed for the smart fin. The remarkable results from those analysis is that the flutter would occur with the flight speed a little higher than the aimed flight speed of Mach 0.6. The flutter speed is actually expected to be less than the current results, because 'glue' condition is applied between the airfoil shell and the support part. It means that the smart fin has aeroelastically unstable potential with a little stability margin. The plant of the closed-loop control system of the smart fin is obtained from ZAERO. Based on the plant, closed-loop control system is constructed in two independent ways, one of which is to use ZAERO for observing flutter boundary, and the other is to use MATLAB/Simulink for observing the time simulations. A controller for the closed-loop control system analysis using ZAERO is designed based on the classic control theory. This controller helps the flutter speed of the smart fin to be 24% greater than before when the controller is added. For the closed-loop control system in MATLAB/Simulink, the input of the pitch angle of the smart fin is saturated, due to the limitation of the applied voltage. Another controller is applied the closed-loop control system built in MATLAB/Simulink. The second controller is designed to decrease the settling time, so satisfies the requirement of the smart fin, as showing that the settling time is lower than 0.1 second. In the present thesis, the controllers used in ZAERO and MATLAB/Simulink improve the flutter boundary and the settling time, respectively.

V. Future Works

Although the piezoelectric actuator, produces the pitch angle of 10°, is not applied in this thesis, the research process for control of the flight dynamics is suggested. As the further future work, study of the only piezoelectric actuator can be proposed. In addition to 3203HD, applied in this thesis, there is PMN-29PT, which has probability to produce larger deflection. It is realized that PMN-29PT has improved piezoelectrically induced strain. For this reason, PMN-29PT can be also applied to an actuator for producing larger deflection in the futures. Additionally, robust and developed controller can be designed, which can covers the total region of the flight speed and overcomes the external disturbances such as gust.

Reference

[1] Bisplinghoff, R. L., Raymond, L., Ashley, H., Halfman, Robert, L., Aeroelasticity. Addison-Wesley Publications, Massachusetts, 1957.

[2] Collar, A. R., “The Expanding Domain of Aeroelasticity,” Royal Aeronautical Society Journal, Vol. 50, Aug. 1946, pp. 613~636.

[3] Bisplinghoff, R. L., and Ashley, H., Principles of Aeroelasticity, 1st ed., Wiley, New York, 1962, pp. 18–69.

[4] Collar, A. R., “The Expanding Domain of Aeroelasticity,” Royal Aeronautical Society Journal, Vol. 50, Aug. 1946, pp. 613~636.

[5] Mehmet, O. N., “Aeroservoelastic Modeling of a Missile Control Fin,” Master’s Thesis, Middle East Technical University, 2013.

[6] Garrick, I. E., “Aeroelasticity-Frontiers and Beyond,” Journal of Aircraft, Vol. 13, No. 9, 1976, pp. 641~657.

[7] Yoon, K. J., Yoon, B. S., “Design/Fabrication/Performance Test of UAV Actuator S-LIPCA with PMN-29PT Piezo-electric Single Crystal,” Journal of the KSAS, No. 11, 2013, pp. 985~988.

[8] Jaffe, B., Cook, W. R. Jr., and Jaffe, H., “Piezoelectric Ceramics”, Academic Press London and New York, 1971.

[9] Crawley, E. F., Luis J., “Use of Piezoelectric Actuators as Elements of Intelligent Structures”, AIAA Journal, Vol. 25, No. 10, 1987, pp. 1373~1385.

[10] Barrett, R., “Aeroservoelastic DAP Missile Fin Development,” Smart Materials and Structures, Vol. 2, No. 2, 1993, pp. 55~65.

[11] Mani, S., Singh, S. N., Parimi, S. K., Yim, W., Trabia, M., "Adaptive Control of a Projectile Fin Using Piezoelectric Elastic Beam," AIAA Guidance, Navigation, and Control Conference and Exhibit, University of Nevada, Las Vegas, 2005.

[12] Park, H. C., Adyatama, P., Lee, H. Y., "A Single-Crystal PMN-29PT Stack Actuator: Fabrication and Performance," Journal of the Korean Ceramic Society, Vol. 50, No. 6, 2013, pp. 545~550.

[13] Ohanian, Ⅲ O., Hickling, C., Stiltner, B., "Piezoelectric Morphing versus Servo-Actuated MAV Control Surfaces," 53rd AIAA/ASME/ASCE/AHS/ASC Structures, Structural Dynamic and Materials Conference, Honolulu, 2012.

[14] Sahin, M., "Smart Structures and Their Applications on Active Vibration Control: Studies in the Department of Aerospace Engineering, METU," Journal of Electroceramics, Vol. 20, Issue 3~4, 2008, pp. 167~174.

[15] Park, C. W., Chung, C. H., Kang, Y. J., Shin, S. J., Yoon, B. S., Park, J. H., Yoon, K. J., "Structural Analysis of Smart Fins Operated by Piezoelectric Actuators for Performance Improvement," International Conference on Adaptive Structures and Technologies, Japan, 2015.

[16] ZAERO Theoretical Manual Version 9.0, Twenty-third Edition, ZONA Technology., Arizona, USA, 2015.

[17] Chen, P. C., "A Damping Perturbation Method for Flutter Solution: The g-Method," International Forum on Aeroelasticity and Structural Dynamics, Hampton, VA, Jun. 22-25, 1999. Also in AIAA Journal, Vol. 38, No. 9, Sep 2000, pp. 1519-1524.

[18] Roger, K. L., "Airplane Math Modeling and Active Aeroelastic Control Design," AGARD-CP-228, 1977, pp. 4.1~4.11.

[19] Karpel, M., “Design for Active and Passive Flutter Suppression and Gust Alleviation,” NASA-CR-3482, 1981.

[20] Park. C. W., Kang. Y. J., Shin. S. J., Yoon. B. S., Yoon. K. J., “CFD-CSD Coupled Analysis of Smart Fins Operated by Piezoelectric Actuators,” KSAS 2016 Spring Conference, Dae Myung Resort Delpino, Seorak, 2016.

[21] Liu, D. D., Chen, P. C., Yao, Z. X., Sarhaddi, D., “Recent Advances in Lifting Surface Methods,” The Aeronautical Journal, Royal Aeronautical Society, Vol. 100, No. 998, Oct. 1996, pp. 327~339.

국문 초록

성능 개선을 위한 압전재료 구동 지능형 조종익의 PI 제어기 설계 및 서보공력탄성학 해석

강 유 진

기계항공공학부

서울대학교 대학원

한 가벼운 비행체에, 압전재료와 같은 지능 재료로 이루어진 작동기가 조종면을 작동시키기 위해 사용되고 있다. 작동기 안의 압전재료 물질에 전압 차가 적용이 되면 스스로 변형을 일으켜 피치 모멘트를 형성함으로써 그 조종면의 피치 각도를 조절한다. 그러한 조종면을 지능형 조종익이라고 부른다. 본 논문에서는 정적 변형 예측과 모드 해석 등 구조 해석을 시작으로, 공력탄성학적 특성과 제어기와 조종면에 의한 서보공력탄성학적 안정성을 예측하고 지능형 조종익 조종 시스템의 시간영역 구조 반응 시뮬레이션을 구축하였다. 주로, MSC.NASTRAN, ZAERO, 그리고 MATLAB/Simulink 를 활용하여 모든 해석을 수행하였다. 이 과정에서 비행 안정성을 보장하고 특정 비행 조건에서 피치 각도를 유지할 수 있게 하는 PI 제어기가 설계되었고, 전체적인 지능형 조종익 조종 시스템의 폐루프는 ZAERO 와 MATLAB/Simulink 에서 각각 다른 두 가지 목적으로 설립되었다. ZAERO 에서 설립된 폐루프 안의 제어기는 지능혀 조종익의 플러터 경계를 높였고, MATLAB/Simulink 에서 설립된 폐루프 안의 제어기는 스텝 함수

모양의 조종면 입력 신호에 대한 구조 응답 시뮬레이션의 정정 시간을 줄임으로써 목표 비행속도 하에서 지능형 조종익의 조종 성능을 개선하였다.

주요어 : 지능형 조종익, 압전재료, 유리함수 근사법, 공력탄성학, 플러터, 서보공력탄성학, PI 제어기, MATLAB/Simulink, ZAERO, 모드 해석

학 번 : 2014-22507